Common effect of chemical and external pressures on the magnetic properties of RCoPO (R = La, Pr)

Common effect of chemical and external pressures on the magnetic properties of *R*CoPO (*R* = La, Pr)

G. Prando,[1,*] P. Bonfà,[2] G. Profeta,[3] R. Khasanov,[4] F. Bernardini,[5] M. Mazzani,[2] E. M. Brüning,[1] A. Pal,[6] V. P. S. Awana,[6] H.-J. Grafe,[1] B. Büchner,[1,7] R. De Renzi,[2] P. Carretta,[8] and S. Sanna[8]

[1]*Leibniz-Institut für Festkörper- und Werkstoffforschung (IFW) Dresden, D-01171 Dresden, Germany*
[2]*Dipartimento di Fisica and Unità CNISM di Parma, Università di Parma, I-43124 Parma, Italy*
[3]*Department of Physical and Chemical Sciences and SPIN-CNR, Università dell'Aquila, I-67100 L'Aquila, Italy*
[4]*Laboratory for Muon Spin Spectroscopy, Paul Scherrer Institut, CH-5232 Villigen PSI, Switzerland*
[5]*IOM-CNR and Dipartimento di Fisica, Università di Cagliari, I-09042 Monserrato (Ca), Italy*
[6]*National Physical Laboratory (CSIR), New Delhi 110012, India*
[7]*Institut für Festkörperphysik, Technische Universität Dresden, D-01062 Dresden, Germany*
[8]*Dipartimento di Fisica and Unità CNISM di Pavia, Università di Pavia, I-27100 Pavia, Italy*

(Received 19 December 2012; revised manuscript received 19 January 2013; published 1 February 2013)

We report a detailed investigation of *R*CoPO (R = La, Pr) and LaCoAsO materials performed by means of muon spin spectroscopy. Zero-field measurements show that the electrons localized on the Pr^{3+} ions do not play any role in the static magnetic properties of the compounds. Magnetism at the local level is indeed fully dominated by the weakly itinerant ferromagnetism from the Co sublattice only. The increase of the chemical pressure triggered by the different ionic radii of La^{3+} and Pr^{3+}, on the other hand, plays a crucial role in enhancing the value of the magnetic critical temperature and can be mimicked by the application of external hydrostatic pressure up to 24 kbar. A sharp discontinuity in the local magnetic field at the muon site in LaCoPO at around 5 kbar suggests a sizable modification in the band structure of the material upon increasing pressure. This scenario is qualitatively supported by *ab initio* density-functional-theory calculations.

DOI: 10.1103/PhysRevB.87.064401 PACS number(s): 74.70.Xa, 71.15.Ap, 75.50.Cc, 76.75.+i

I. INTRODUCTION

The discovery of high-T_c superconductivity in F-doped *R*FeAsO (1111) was one of the most significant breakthroughs in the field of condensed matter physics during the last decades.[1,2] A striking worldwide interest has been indeed recently devoted to the synthesis of this class of materials, looking for suitable chemical substitutions of rare-earth (R) ions, transition metals (TM), and pnictogen elements (Pn) allowing one to enhance the critical temperature T_c, the highest value $T_c \simeq 55$ K being currently reached in $SmFeAsO_{1-x}F_x$.[2–4] Electron doping can be realized directly on the FeAs layers also leading in turn to superconductivity. In this respect, one of the most studied chemical substitutions of TM is $Fe_{1-x}Co_x$. This applies to Fe-based materials belonging both to 1111 and to 122 families, the parent compound for the latter case being $BaFe_2As_2$.[5–12]

Beyond superconductivity, 1111 materials show interesting magnetic features associated with the mutual interaction among localized electrons onto the external shells of R ions and itinerant carriers from the TM sublattice.[13] A strong f-d hybridization was shown to be present, for instance, in superconducting $SmFeAsO_{1-x}F_x$ under conditions of optimal doping.[14] In the case of undoped *R*FeAsO compounds, a spin density wave (SDW) phase below $T_N \simeq 140$ K associated with itinerant d electrons from Fe is found to coexist with an antiferromagnetically (AFM) ordered phase of R magnetic moments at much lower temperatures ($T_N^R \sim 5$–10 K).[15,16] It should be stressed how the full substitution of Fe by Co has attracted particular interest, e.g., in *R*CoAsO compounds where much more complex magnetic behaviors were shown by means of both macroscopic and local experimental techniques.[17–26] The Co sublattice, in particular, is known to enter a weakly itinerant ferromagnetic (FM) phase below $T_C \simeq 60$–80 K, the precise value of T_C being strongly dependent on R.[17,19,20,25,26] At lower temperatures, the occurrence of other phase transitions is clearly observed in samples containing magnetic R ions as a consequence of the strong interaction among the two magnetic sublattices. This behavior, in fact, is typically interpreted as the result of progressive FM-AFM transitions of the Co sublattice induced by the R ions followed at the lowest temperatures by the full magnetic ordering of the R sublattice.[19,20,25,26]

A similar phenomenology has been recently reported in the isostructural P-based *R*CoPO compounds.[17,27,28] LaCoPO has been investigated by means of ^{31}P nuclear magnetic resonance (NMR) showing that Moriya's theory of self-consistently renormalized spin fluctuations for weakly itinerant magnets ($T_C \simeq 35$ K) well describes the experimental results.[29–31] Magnetotransport, dc magnetometry, and NMR measurements on compounds with magnetic R ions such as Sm^{3+} and Nd^{3+} show the occurrence of multiple magnetic phase transitions similarly to the case of *R*CoAsO.[28,32] In *R*CoPO compounds, an interaction between the two magnetic sublattices much stronger than what is occurring in *R*CoAsO should be expected. The P/As isovalent substitution for the Pn element, in fact, is known to introduce a strong chemical pressure making the R ions much closer to the itinerant layers. In the case of $CeFeAs_{1-x}P_xO$, for instance, these effects are known to gradually suppress the SDW phase associated with Fe upon increasing x, driving at the same time the R sublattice from an AFM ordered phase through a FM ground state (GS) and finally towards a Kondo-screened phase where heavy-fermion phenomenology is recovered.[33–36]

In order to evidence how crucial the role of the chemical pressure on the magnetic properties of *R*CoPO materials is, we performed measurements of muon spin spectroscopy on these compounds. In this paper, we report on the results obtained in LaCoPO and PrCoPO, where the local magnetism was investigated upon the application of external hydrostatic pressure up to 24 kbar. Remarkably, in spite of the high value of the magnetic moment expected for the free Pr^{3+} ion ($\mu_{Pr} \simeq 3.6\ \mu_B$), electrons localized on the external shells of Pr^{3+} do not play any role in the local static magnetic properties of PrCoPO probed by muons. For both compounds, only the itinerant ferromagnetism from the Co bands dominates the observed response. The chemical pressure triggered by the full Pr^{3+}/La^{3+} substitution, on the other hand, has a sizable effect in enhancing the value of the critical temperature of the itinerant ferromagnetic phase. In this respect, external hydrostatic pressure is shown to lead to the same result as Pr/La substitution both in LaCoPO and, to a lesser extent, in the isostructural compound LaCoAsO. Furthermore, both chemical and external pressures strongly suppress the local magnetic field at the muon site while leaving the magnetic moment per Co ion substantially unchanged. It should be remarked that the chemical shrinkage of the lattice is intrinsically expected to be characterized by a higher degree of nonhydrostaticity that, in the case of 122 systems, was shown to play a drastic role in governing the resulting magnetic properties.[37] However, claims of close analogies among the effect of chemical and external pressures were reported concerning both 1111 and 122 compounds.[38–40] The results presented in this paper further confirm this latter scenario also for Co-based 1111 materials. *Ab initio* density-functional-theory calculations have been developed to describe the effects of pressure both on the interstitial crystallographic sites for the muons and on the electronic bands of LaCoPO. Results support the experimental findings and suggest that chemical and external pressures can both trigger a change in the electronic band structure. As a remarkable output, chemical and external hydrostatic pressures act similarly on the magnetic properties of LaCoPO.

II. EXPERIMENTAL DETAILS

Loose powders of LaCoAsO, LaCoPO, and PrCoPO were grown via solid-state reactions as described in detail in Refs. 24 and 28. The structural properties of the lattices were measured at room temperature by means of a Rigaku x-ray diffractometer with Cu K_α radiation. The Rietveld analysis of the diffraction patterns (see Fig. 1) confirmed that all the samples crystallized in the tetragonal phase, space group $P4/nmm$, and allowed us to extract the values of the lattice parameters a and c (see Table I). It is clear from Table I how both the P/As and Pr/La substitutions increase the chemical shrinkage of the cell and reduce both a and c accordingly. This is in agreement with what is generally reported for all the 1111 family of compounds.[19,34,41]

Measurements of zero-magnetic-field (ZF) muon spin spectroscopy (μ^+SR) were performed at the GPD spectrometer (μE1 beamline) of the SμS muon source at the Paul Scherrer Institut, Switzerland (see Ref. 42 for a comprehensive introduction to μ^+SR techniques). Pressure (P) was applied at ambient temperature (T) in a double-wall piston-cylinder

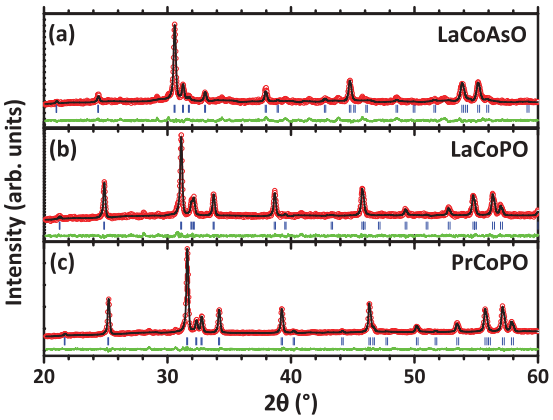

FIG. 1. (Color online) Observed (red circles) and calculated (blue solid lines) x-ray powder-diffraction patterns at room temperature for the investigated samples of LaCoAsO [see (a) panel], LaCoPO [see (b) panel]. and PrCoPO [see (c) panel]. Black lines are best fits to experimental data according to a Rietveld analysis.

cell made of MP35N alloy and its value was quantified by ac susceptometry at $T \sim 3$ K from the shift of the superconducting critical temperature of a small In wire inside the cell. The transmitting medium Daphne oil 7373 was employed assuring that the pressure conditions were always nearly hydrostatic in the experimental range.[43,44] The maximum P value attainable at low T with this setup is close to 24 kbar. The pressure cell (PC) intrinsically leads to an extremely high-background level in ZF-μ^+SR measurements, whose behavior as a function of T was tested and measured in an independent set of experiments. For this reason, a ZF-μ^+SR characterization of the samples was also performed at the low-background spectrometers Dolly and GPS (πE1 and πM3 beamlines, respectively) at PSI.

The dc magnetization measurements were performed by using the commercial superconducting quantum interference device (SQUID) magnetometer MPMS-XL7 (Quantum Design). A piston-cylinder CuBe PC (EasyLab Mcell 10) was used to apply hydrostatic $P \leqslant 11$ kbar. Again, the Daphne oil 7373 was employed as transmitting medium. P was applied at ambient T and its value quantified at low T from the shift of the superconducting critical temperature of a small Sn wire inside the cell.

III. EXPERIMENTAL RESULTS

The measured spin-depolarization functions for the implanted muons (μ^+) as a function of time (t) in ZF conditions were fitted for all the samples and at all the investigated

TABLE I. Lattice parameters for the investigated samples after Rietveld refinements of x-ray powder diffraction patterns displayed in Fig. 1.

Compound	a (Å)	c (Å)	Volume (Å^3)	χ^2
LaCoAsO	4.048(8)	8.462(7)	138.73(1)	3.32
LaCoPO	3.966(7)	8.365(0)	131.62(7)	2.12
PrCoPO	3.9208(4)	8.212(4)	126.25(0)	2.31

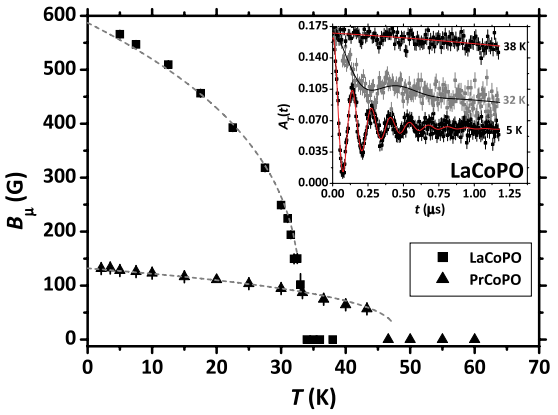

FIG. 2. (Color online) Main experimental results of ZF-μ^+SR (ambient P, Dolly spectrometer). Main panel: B_μ vs. T for LaCoPO and PrCoPO. Dashed lines are best-fits to experimental data according to Eq. (3). Inset: raw ZF spin-depolarization data for LaCoPO at some selected T values. Continuous lines are best fits to experimental data according to Eq. (1), where $a_{PC} = 0$.

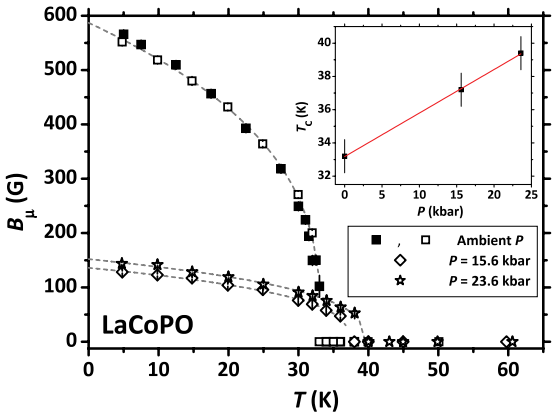

FIG. 3. (Color online) Main panel: $B_\mu(T)$ at different P for LaCoPO. Dashed lines are best fits to experimental data according to Eq. (3) with $\beta = 0.34$ as fixed parameter. Closed and open symbols for ambient P data refer to measurements performed at Dolly and at GPD with unloaded cell, respectively. Inset: T_C vs P. The continuous line is a best fit to data according to a linear function.

T values by the general expression

$$A_T(t) = A_0\left[a_{PC}\, e^{-\frac{\sigma_{PC}^2 t^2}{2}} + (1 - a_{PC})G_T^s(t)\right]. \quad (1)$$

Here, the amplitude a_{PC} accounts for the fraction of incoming μ^+ stopping in the PC. The depolarization of these μ^+ is a Gaussian-type relaxation governed by a nearly T-independent σ_{PC} term arising from nuclear magnetism inside the MP35N alloy. The remaining fraction $(1 - a_{PC})$ of μ^+ is implanted directly into the sample and, accordingly, the relative depolarization $G_T^s(t)$ can be described as

$$G_T^s(t) = [1 - V_m(T)]e^{-\frac{\sigma_N^2 t^2}{2}} + [a^\perp(T)F(t)D^\perp(t) + a^\parallel(T)D^\parallel(t)]. \quad (2)$$

Here, the quantity $V_m(T)$ represents the fraction of μ^+ experiencing a static local magnetic field or, equivalently, the magnetic volume fraction of the investigated sample. In the paramagnetic limit, namely, $V_m(T) = 0$, no static field of electronic origin contributes to the depolarization and only the weak contribution from the nuclear magnetic moments leads to a slow Gaussian depolarization with characteristic rate σ_N (typical measured values $\sigma_N \sim 0.1\ \mu s^{-1}$). Below the magnetic-order critical transition temperature T_C, the superscript $\perp$ ($\parallel$) refers to μ^+ experiencing a local static magnetic field in a perpendicular (parallel) direction with respect to the initial μ^+ spin polarization. The amplitudes $a^{\perp,\parallel}$ must then satisfy the condition $[a^\perp(T) + a^\parallel(T)] = V_m(T)$ accordingly. In the presence of a long-range magnetic order inside the sample, a coherent precession of μ^+ around the local magnetic field B_μ can be discerned in the $a^\perp$ amplitude and described by the oscillating function $F(t)$. The (either exponential or Gaussian) damping function $D^\perp(t)$ reflects a distribution of local magnetic field values at the μ^+ site. The $a^\parallel$ component, on the other hand, is typically damped by the exponentially decaying function $D^\parallel(t) = e^{-\lambda^\parallel t}$ probing spin-lattice-like relaxation processes ($\lambda^\parallel \sim 0.1\ \mu s^{-1}$).

Standard oscillating functions $F(t) = \cos(\gamma B_\mu t + \phi)$, where $\gamma = 2\pi \times 135.54$ MHz/T is the magnetogyric ratio for μ^+, are in good agreement with experimental data (statistical $\chi^2 \simeq 1$–1.2). Negative values for the phase $|\phi| \sim 20^\circ$–30° were systematically measured at the low-background spectrometer Dolly, similarly to what was reported in literature for RCoAsO compounds.[26] Phase values close to -30° can be considered an experimental proof of magnetically ordered phases incommensurate with the underlying crystalline lattice. This case is typically handled by putting $F(t) = J_0(\gamma B_\mu t)$ where J_0 is a first-kind zeroth-order Bessel function.[45] However, not always is this enough as an unambiguous evidence of incommensurability. As suggested in Ref. 26, for instance, a systematic instrumental delay in the data acquisition can also explain the observed behavior.

The three main contributions to the local field at the muon site B_μ in the case of ferromagnetic materials come from the dipolar field, the transferred hyperfine field, and the Lorentz field.[46] As it will be discussed in more detail later in Sec. IV [see Eq. (4)], the crucial physical parameters governing the amount of those contributions are the distance between the μ^+ and the magnetic ions, the magnetic moment of the ordered magnetic phase, and the density of spins at the μ^+ site.[47] Once the interstitial crystallographic position of the μ^+ is known, the independent knowledge of the value of the magnetic moment (by means of, e.g., dc magnetometry) is of crucial importance since it allows one to directly access the transferred hyperfine field.[46,47]

Representative ZF μ^+ depolarizations for LaCoPO obtained at Dolly (ambient P) are presented in the inset of Fig. 2. Coherent oscillations indicative of the establishment of a long-range magnetic order can be clearly discerned for $T \leqslant T_C \simeq 33$ K down to the lowest investigated temperature. Experimental data were fitted by means of Eq. (1) accordingly, where $a_{PC} = 0$. The T dependence of the magnetic volume fraction V_m (not shown) confirms that the sample is fully magnetic below T_C. The B_μ versus T trend is plotted in the main panel of Fig. 2 and can be fitted according to a power-law function

$$B_\mu(T) = B_\mu(0)\left(1 - \frac{T}{T_C}\right)^\beta \quad (3)$$

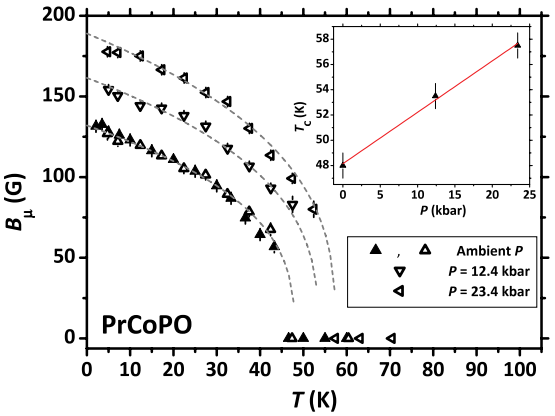

FIG. 4. (Color online) Main panel: $B_\mu(T)$ at different P for PrCoPO. Dashed lines are best fits to experimental data according to Eq. (3) with $\beta = 0.34$ as fixed parameter. Closed and open symbols for ambient P data refer to measurements performed at Dolly and at GPD with unloaded cell, respectively. Inset: T_C vs P. The continuous line is a best fit to data according to a linear function.

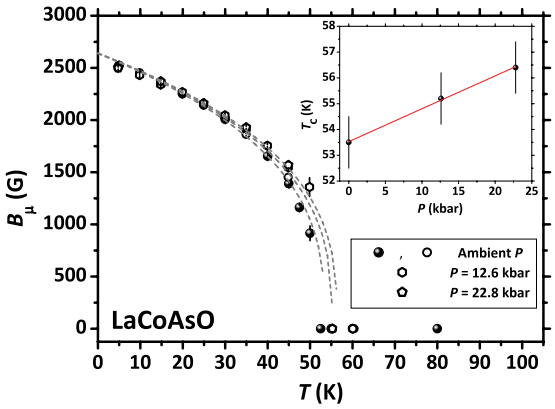

FIG. 5. (Color online) Main panel: $B_\mu(T)$ at different P for LaCoAsO. Dashed lines are best fits to experimental data according to Eq. (3) with $\beta = 0.34$ as fixed parameter. Closed and open symbols for ambient P data refer to measurements performed at Dolly and at GPD with unloaded cell, respectively. Inset: T_C vs P. The continuous line is a best fit to data according to a linear function.

eventually saturating at $B_\mu(0) = 587.5 \pm 2.5$ G, the exponent turning out to be $\beta = 0.34 \pm 0.01$.

Also in the case of PrCoPO, measurements performed at Dolly reveal a static long-range magnetism probed by μ^+ in 100% of the magnetic volume (not shown) below $T_C \simeq 48$ K. The value for T_C is sizably increased with respect to what is observed in LaCoPO, consistently with what is reported for RCoAsO compounds.[26] Remarkably, the B_μ versus T trend still can be well described by Eq. (3) where again $\beta = 0.34 \pm 0.01$ (see the main panel of Fig. 2). In the case of PrCoPO, only the local field $B_\mu(0) = 132 \pm 2$ G is more than four times lower than in LaCoPO. In spite of the high value for the localized magnetic moment expected for the free Pr^{3+} ion ($\sim$3.6 μ_B), the results for the PrCoPO sample are qualitatively identical to the case of LaCoPO. This is clearly different from what was previously reported in the literature for the As-based compound PrCoAsO, where a more complex phenomenology for ZF-μ^+SR (displaying a splitting of internal fields) was observed.[26] Nevertheless, dc magnetization measurements for LaCoAsO and PrCoAsO were reported to display no sizable differences among themselves, no anomalies being detected for $T \leqslant T_C$.[26] The present results (together with what is reported in Ref. 26) then suggest that both in PrCoPO and in PrCoAsO the magnetic moments localized on the Pr^{3+} ions do not play any role in the static magnetic features of these compounds. The phenomenology observed in PrCoAsO (Ref. 26) then can possibly be due to the presence of two different μ^+ sites whose statistical population is strongly dependent on T in the investigated experimental range.

The overall scenario deduced from our measurements on LaCoPO and PrCoPO and from the previous characterization of the materials (see Sec. II) suggests that the main effect of the full Pr/La substitution is only associated with a lattice shrinkage induced by the different chemical pressures associated to the different ionic radii of La^{3+} and Pr^{3+}. This is different from the cases of all other magnetic R ions where the interplay of the localized and the itinerant magnetic degrees of freedom leads to progressive FM-AFM reordering effects on the Co sublattice. Therefore, it seems safe to deduce that Pr^{3+} magnetic moments do not contribute to the local static magnetic properties of the compound that are only governed by weakly itinerant FM from Co.

The validity of these arguments is corroborated by the measurements under external P performed at the GPD spectrometer. In spite of the fact that almost half of the incoming μ^+ stop inside the pressure cell ($a_{PC} \sim 0.5$), clear oscillations can be distinguished from the ZF signal associated with all the samples below characteristic critical transition temperatures $T_C(P)$. The analysis of V_m (not shown) clearly shows that the magnetic phase is extended over the whole sample volume independently on the P value for all the investigated materials. The T dependence of B_μ for the three samples at different values of P are reported in the main panels of Figs. 3–5 (LaCoPO, PrCoPO, and LaCoAsO, respectively). Here, the T_C values are estimated as free parameters from the fitting to experimental ZF data according to Eq. (3) where, in view of the results of ambient pressure measurements, $\beta = 0.34$ is kept as a fixed parameter for all the samples.

By focusing on the results for LaCoPO first and by comparing the main panels of Figs. 2 and 3, it is immediate to realize that the qualitative effect of increasing P is extremely similar to what is induced by the full Pr/La substitution. In particular, a strong suppression of $B_\mu(0)$ together with a sizable enhancement of T_C are obtained at the maximum applied $P \simeq 23.6$ kbar. As shown by the dashed lines in the main panel of Fig. 3, the fitting function reported in Eq. (3) still well reproduces the observed experimental data with $\beta = 0.34$ at all the P values. By more carefully investigating the experimental results reported in Fig. 3, one realizes that the suppression of B_μ is actually nonmonotonic with increasing P (see also Fig. 8 later on). Remarkably, this sharp jump in the internal magnetic field is not reflected in the P dependence of T_C that steadily increases in a linear fashion across the whole experimental range (see the inset of Fig. 3). Quantitative data relative to the linear increase of T_C as a function of P are reported in Table II.

As already shown in Fig. 2 for the measurements at ambient P, the T dependence of B_μ in PrCoPO is qualitatively identical

TABLE II. Summarizing quantities of interest for the three investigated compounds after ZF-μ^+SR measurements under P. $T_C(0)$ represents the critical temperature at ambient P while $\left(\frac{dT_C}{dP}\right)$ is the slope of the linear trends of T_C versus P presented in the insets of Figs. 3, 4, and 5.

Compound	$T_C(0)$ (K)	$\left(\frac{1}{T_C(0)}\right)\cdot\left(\frac{dT_C}{dP}\right)$ (kbar^{-1})
LaCoAsO	53.5 ± 1.0	$(2.35 \pm 0.15) \times 10^{-3}$
LaCoPO	33.2 ± 1.0	$(8.0 \pm 0.5) \times 10^{-3}$
PrCoPO	48.0 ± 1.0	$(8.5 \pm 0.5) \times 10^{-3}$

to what it is reported for LaCoPO. Remarkably, measurements performed at GPD (reported in Fig. 4) confirm this qualitative result also for P values up to 23.4 kbar. As it is found in the case of LaCoPO, a linear increase of T_C as a function of P can be inferred (see the inset of Fig. 4 and Table II). However, differently from LaCoPO, the saturation value of the internal field $B_\mu(0)$ is steadily enhanced upon increasing P, reaching $B_\mu(0) \simeq 189$ G at the maximum P value (see also Fig. 8 later on).

A totally different phenomenology is detected for LaCoAsO up to the value $P = 22.8$ kbar. As it is clear from Fig. 5, the value $B_\mu(0) \simeq 2640$ G does not display any dependence upon P within the experimental error, while the linear increase of T_C is much less marked than in the case of LaCoPO and PrCoPO (see Table II). It should be remarked that, as it is discussed in detail later in Sec. IV, the sizable difference of $B_\mu(0)$ between the case of P- and As-based samples can be explained by the preferential occupation of different crystallographic sites by the muons in the two cases [close to LaO and Co(Pn) trilayers, respectively]. However, the function reported in Eq. (3) still yields to good fitting results for $B_\mu(T)$ data with $\beta = 0.34$ as a fixed parameter independently on the P value. Since both the materials with La as nonmagnetic R ion then share the same power-law-like trend, it is further confirmed that this must be entirely associated to the Co sublattice. It seems safe to deduce that this behavior for $B_\mu(T)$ is the fingerprint of static magnetism from Co in RCo(As,P)O

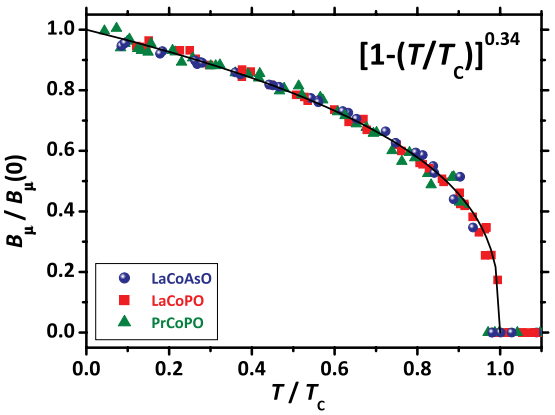

FIG. 6. (Color online) B_μ vs T for the three samples at all the investigated P values. Data clearly collapse on a single common power-law-like trend with $\beta = 0.34$ (continuous line) after a proper scaling of both T and B_μ axes with T_C and $B_\mu(0)$ values, respectively.

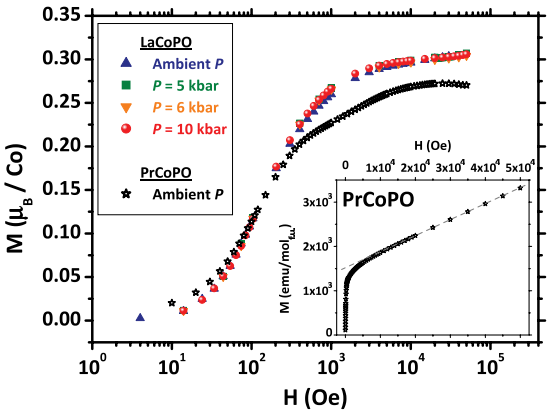

FIG. 7. (Color online) Main panel: M vs H at fixed $T = 5$ K for LaCoPO at different P values and for PrCoPO at ambient pressure after the subtraction of the linear paramagnetic term due to Pr^{3+} ions. Inset: raw magnetization data for PrCoPO before the subtraction of the linear paramagnetic term evidenced by the dashed line.

materials. Data at ambient P are in good agreement with what was previously reported in the literature.[26]

In order to stress the strong qualitative analogies among the three investigated samples, the experimental data displaying B_μ versus T at all the different P values are plotted in Fig. 6. Here, a scaling procedure along both the T and B_μ axes with, respectively, T_C and $B_\mu(0)$ values proper of each data set allows us to clearly enlighten a shared power-law-like trend with exponent $\beta = 0.34$ common to all the samples and independent on P.

As already commented above (and as further discussed in detail later in Sec. IV), the relative variations of B_μ in ferromagnets can not be ascribed only to variations in the value of the magnetic moment in the ordered phase, and a further experimental study for such quantity should be independently performed. To this aim, the behavior of μ_{Co} versus P in LaCoPO was investigated in the low-P region by means of dc magnetometry. Measurements of dc magnetization (M) as a function of the magnetic field (H) were performed at $T = 5$ K up to $P = 10$ kbar. The results are reported in the main panel of Fig. 7. The unique intrinsic contribution to M in LaCoPO is expected to come from the weakly itinerant FM state associated with the Co sublattice and an ordered value of $\mu_{Co}^{LaCoPO} = 0.3 \pm 0.02\ \mu_B$ can be indeed estimated, in good agreement with previous reports.[17,28] Remarkably, μ_{Co}^{LaCoPO} turns out to be independent on P within the experimental error in the investigated P range. The same scenario holds for PrCoPO, as it is deduced from M versus H measurements at ambient P (raw data are presented in the inset of Fig. 7). After the subtraction of the linear term enlightened in the inset of Fig. 7 by means of a dashed line and accounting for the paramagnetic contribution of Pr^{3+} magnetic moments, one obtains the intrinsic contribution of the Co sublattice reported in the main panel of Fig. 7. Results only show a slight reduction of the magnetic moment of Co in PrCoPO with respect to what was found for LaCoPO ($\mu_{Co}^{PrCoPO} = 0.275 \pm 0.025\ \mu_B$ should be compared with $\mu_{Co}^{LaCoPO} = 0.3 \pm 0.02\ \mu_B$). These results clearly indicate that the dramatic drop in $B_\mu(P)$ described in the main panel of Fig. 3 can not be ascribed to a sudden suppression of μ_{Co}.

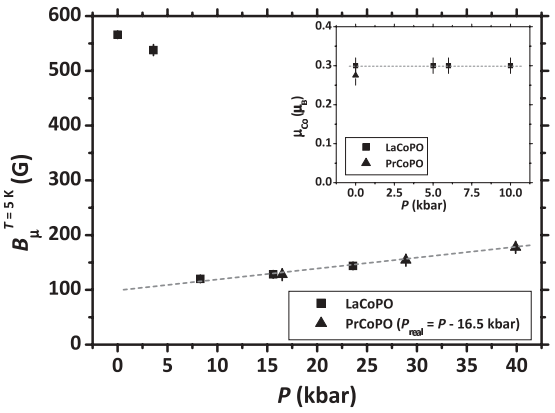

FIG. 8. Main panel: B_μ vs P at $T = 5$ K for both LaCoPO and PrCoPO. A biasing value $P_B = 16.5$ kbar was added to real P values for PrCoPO. The dashed line is a linear guide for the eye. Inset: values of μ_{Co} deduced for LaCoPO and PrCoPO from the dc magnetization measurements presented in Fig. 7. The dashed line is a guide for the eye.

A summary of the main experimental results for B_μ versus P in LaCoPO and PrCoPO at $T = 5$ K is reported in the main panel of Fig. 8. Data already reported in Fig. 3 for LaCoPO have been complemented by two single measurements at $T = 5$ K and at low P values ($\sim$3 and $\sim$8 kbar). This allows us to confirm the reproducibility of the dramatic reduction of B_μ and to characterize it as a sudden phenomenon occurring in a window with maximum width of few kbar around $P \sim 5$ kbar. Data for PrCoPO, on the other hand, have been plotted in the main panel of Fig. 8 after adding a phenomenological biasing pressure $P_B = +16.5$ kbar. It is interesting to notice that, after such shift along the P axis, a systematic common enhancement of B_μ with increasing P can be clearly discerned sharing the same slope (1.95 ± 0.05 G/kbar) for the two different materials. Naively, one can think of P_B as an effective pressure equivalent to the internal chemical pressure associated with the full Pr/La substitution. The inset of Fig. 8 summarizes the behavior of μ_{Co} versus P as determined by dc magnetization measurements. It is clear how, in the range of P values up to 10 kbar, the value of μ_{Co} is indeed constant and approximately equal to 0.3 μ_B.

Modifications of contributions to the local field other than the dipolar coupling among μ^+ and Co layers should then be responsible for the observed behavior. This topic will be discussed in more detail in Sec. IV from a computational point of view. In particular, it will be shown how a sizable effect of P in modifying the band structure and, accordingly, the transferred hyperfine term to the μ^+ must be taken into consideration in order to explain the observed behavior.

IV. INSIGHTS INTO THE INTERNAL FIELD AT THE MUON SITE FROM FIRST-PRINCIPLES CALCULATIONS

In this section, we will discuss the sharp suppression of $B_\mu(P)$ occurring at $P = 5 \pm 2$ kbar in LaCoPO (as presented in the main panel of Fig. 8) by taking into consideration different possibilities explaining its origin. To this aim, one should first write the internal field B_μ at the μ^+ site (the position of which is identified by the vector $\mathbf{r}_\mu$) in a nonmagnetized FM material as a sum of several contributions. In particular, one has

$$B_\mu = |\mathbf{B}_{dip}(\mathbf{r}_\mu) + \mathbf{B}_c(\mathbf{r}_\mu) + \mathbf{B}_L|, \quad (4)$$

where $\mathbf{B}_{dip}(\mathbf{r}_\mu)$ is the dipolar field arising from the atoms within a sphere with diameter smaller than R_{md} (R_{md} being the approximate linear dimension of a magnetic domain), $\mathbf{B}_c(\mathbf{r}_\mu)$ is the contact hyperfine field, and $\mathbf{B}_L$ the Lorentz field. By considering the value $\mu_{Co} \simeq 0.3\ \mu_B$ derived in LaCoPO (the superscript was dropped to the aim of clarity) by means of dc magnetization measurements, it is straightforwardly derived that $|\mathbf{B}_L| = (\frac{4\pi}{3})M_{sat} \simeq 170$ G.

As previously discussed in Sec. III, no modification of μ_{Co} could be discerned in LaCoPO upon increasing the value of the external P. The drop of B_μ measured at $P = 5 \pm 2$ kbar may then only be related to the quantities whose values could still be a function of P, namely, $\mathbf{r}_\mu$ and $\mathbf{B}_c$. In the former case, results would then imply that a change of the μ^+ site is at the origin of the observed discontinuity. Such μ^+ jump could be possibly due either to the lattice undergoing a structural transition or, more generally, to a smoother modification of the electrostatic energy landscape triggered by P inducing a change in the μ^+ preferential site. In this respect, it should be remarked that estimates of the structural parameters as a function of P by means of x-ray diffraction measurements would be of the utmost importance in order to get further information. In the latter case, on the other hand, the sudden modification of the $\mathbf{B}_c$ term could follow from the evolution of the structure of electronic bands upon increasing P. One could also consider other possibilities such as, for instance, a P-induced change in the magnetic GS from, e.g., FM to AFM, or a reorientation of the magnetic configuration in the Co sublattice upon gradually increasing P. Finally, and less interestingly, another possibility is that the experimental findings are the result of the local distortion introduced by μ^+ once thermalized inside the material.

In order to get more insights into the origin of the sharp drop in B_μ versus P as revealed by μ^+SR experiments on LaCoPO, *ab initio* calculations were then carried out in order to check for the reliability of all the scenarios proposed above for the material under investigation. The main objects were the computation as a function of P of the crystallographic sites where μ^+ sit and of the energy-volume curves allowing one to derive the structural and magnetic GSs of the system.

A. Computational details

We used both the plane wave (PW) and the full potential linearized augmented plane waves (FP-LAPW) methods as implemented in the VASP (Ref. 48) and ELK (Ref. 49) packages. The Perdew-Burke-Ernzerhof (PBE) functional was used in order to evaluate the exchange-correlation potential.[50] As for the PW approach, the electron-ion interaction was described by the projector augmented wave (PAW) pseudopotentials method.[51] Electronic convergence was set up at 10^{-6} eV and sampling of the Brillouin zone performed by the

Monkhorst-Pack scheme[52] on a $8 \times 8 \times 4$ grid. A plane-wave cutoff of 600 eV and a Gaussian smearing of 0.02 eV was used throughout. FP-LAPW calculations were carried out using a basis set with $R_{\rm min}^{\rm MT} \times \max(\|k\|) = 7.5$, $R_{\rm min}^{\rm MT}$ being the smallest muffin-tin (MT) radius inside the MT spheres, and $l_{\rm max} = 8$ for the angular momentum expansion in the MTs (for both the wave functions and the potential). The reciprocal space was sampled with the same grid used in the PW approach. A close agreement is observed between the results obtained by means of both the computational methods.

Energy-volume curves were obtained from the PW-based calculations by constant volume energy minimization. The convergence criteria for forces minimization was set to 5×10^{-3} eV/Å, and 10^{-5} eV was used as a threshold for self-consistent electronic cycles. The optimized unit-cell volume at ambient P for LaCoPO is 133.21 Å^3 with lattice parameters $a = 3.966$ Å and $c = 8.468$ Å. In accordance with previous findings,[17] the density-functional-theory (DFT) calculations reproduce the experimental structural parameters with errors $\sim$1%. No anomalies in the energy-volume curves are observed within the explored P range. At the same time, the FM-ordered configuration is the GS for P values up to 100 kbar in agreement with experimental results.[17] The results then suggest that both the crystal structure and the FM configuration as GS are stable against the increase of P in LaCoPO at least in the investigated P range. The calculated value for the magnetic moment $\mu_{\rm Co} = 0.57\ \mu_{\rm B}$ is in agreement with previous calculations.[17] This value is slightly higher than our experimental estimate $\mu_{\rm Co} \simeq 0.3\ \mu_{\rm B}$ and it is substantially unchanged for $P < 40$ kbar while, for higher pressures, the magnetic moment on Co atoms linearly decreases, reaching $0.55\ \mu_{\rm B}$ for $P = 100$ kbar.

B. Interstitial μ^+ sites and their stability against zero-point motion and external pressure

The crystallographic sites where μ^+ stop after thermalization processes may be identified to a first extent by calculating the GS electron density of the bulk material under investigation. The minima of the electrostatic potential consequently obtained are indeed found to provide a correct estimate to this aim.[16] Three inequivalent positions are computed for LaCoPO, whose absolute values of the potential energy are denoted as V_0^i ($i = $ A, B, C) where we conventionally set $V_0^{\rm A} \equiv 0$ eV. Site A (B) is located within the LaO (CoP) trilayers, while site C is aligned with O and Co in-between the different trilayers, as shown in Fig. 9(b). Remarkably, we note that the electrostatic interaction favors site A unlike what is found in RCoAsO and RFeAsO where the interstitial site close to the transition-metal plane is favored.[16,26] More detailed information about the crystallographic positions of the three sites and their evolution upon increasing P is reported in Table III and in Fig. 9. The local magnetic fields at the μ^+ sites $\mathbf{B}_{\rm dip}$ arising from the dipolar contribution of $\mu_{\rm Co} = 0.3\ \mu_{\rm B}$ magnetic moments were also computed and reported in Table III (assuming an undistorted lattice).

Once thermalized, in view of the quite high zero-point (ZP) motion energy for μ^+, the potential minima are not necessarily stable trapping sites. Whether the ZP energy is higher than the potential barrier surrounding a minimum, μ^+ can escape to lower-energy ones. To check if the minima yield stable trapping, we computed the ZP motion by solving the Schrödinger equation for the μ^+ in the electrostatic potential. Then, we inspected the position of the probability maxima for the relative GS wave functions and characterized each μ^+ site by the relative lowest eigenvalue $E_{\rm ZP}$ (see Table III). It should be remarked that a stable trapping site must have a nodeless and well-localized GS. Calculations show that this is clearly the case for sites A and B, while for site C we found a delocalized wave function with a large amplitude around C (resonant state). Moreover, for site C, at variance with the findings for sites A and B, the lowest eigenvalue $E_{\rm ZP}^{\rm C}$ is higher than the energy barrier separating A and C. Under these conditions, all μ^+ stopping in C reach the energetically more favorable minimum A. We can not exclude the presence of a self-trapping mechanism which could, in principle, prevent μ^+ from reaching the lowest-energy site A from minimum C. Anyway, the C site has a so high energy that the fraction of μ^+ stopping there should be negligible. From the above considerations, only A and B minima are eligible as stable μ^+ sites and C will be disregarded in the rest of the discussion.

TABLE III. Crystallographic positions of the interstitial sites A, B, and C at two different values of P. The absolute values of the local magnetic field at A, B, and C arising only from the $\mathbf{B}_{\rm dip}$ contribution in Eq. (4) are reported for two different FM configurations of $\mu_{\rm Co}$. The values of the minima of potential energy for the three sites are denoted by V_0^i, while $E_{\rm ZP}^i$ represents the lower eigenvalue for the ZP motion of μ^+ into the i potential dip (see text). The values for the energy barriers between different sites are denoted as $\Delta_{i,i'}$. All the energy values (V_0^i, $E_{\rm ZP}^i$, and $\Delta_{i,i'}$) are conventionally referred to $V_0^{\rm A}$.

Site	Wyckoff position	x (a), y (a), z (c)	$B_{\rm dip}^{\mu_{\rm Co}\|c}$ (G)	$B_{\rm dip}^{\mu_{\rm Co}\perp c}$ (G)	V_0^i (eV)	$E_{\rm ZP}^i$ (eV)
		Ambient P ($\Delta_{\rm AB} = \Delta_{\rm BC} = 1.42$ eV, $\Delta_{\rm AC} = 1.06$ eV)				
A	$2c$	$\frac{1}{4}\ \frac{1}{4}\ 0.875$	330	170	0	0.45
B	$2c$	$\frac{1}{4}\ \frac{1}{4}\ 0.42$	1100	550	0.27	0.63
C	$4f$	$\frac{3}{4}\ \frac{1}{4} 0.30$	–	–	0.56	1.13
		$P = 30$ kbar ($\Delta_{\rm AB} = \Delta_{\rm BC} = 1.36$ eV, $\Delta_{\rm AC} = 1.08$ eV)				
A	$2c$	$\frac{1}{4}\ \frac{1}{4}\ 0.875$	330	170	0	0.45
B	$2c$	$\frac{1}{4}\ \frac{1}{4}\ 0.42$	1100	550	0.37	0.73
C	$4f$	$\frac{3}{4}\ \frac{1}{4} 0.30$	–	–	0.62	1.22

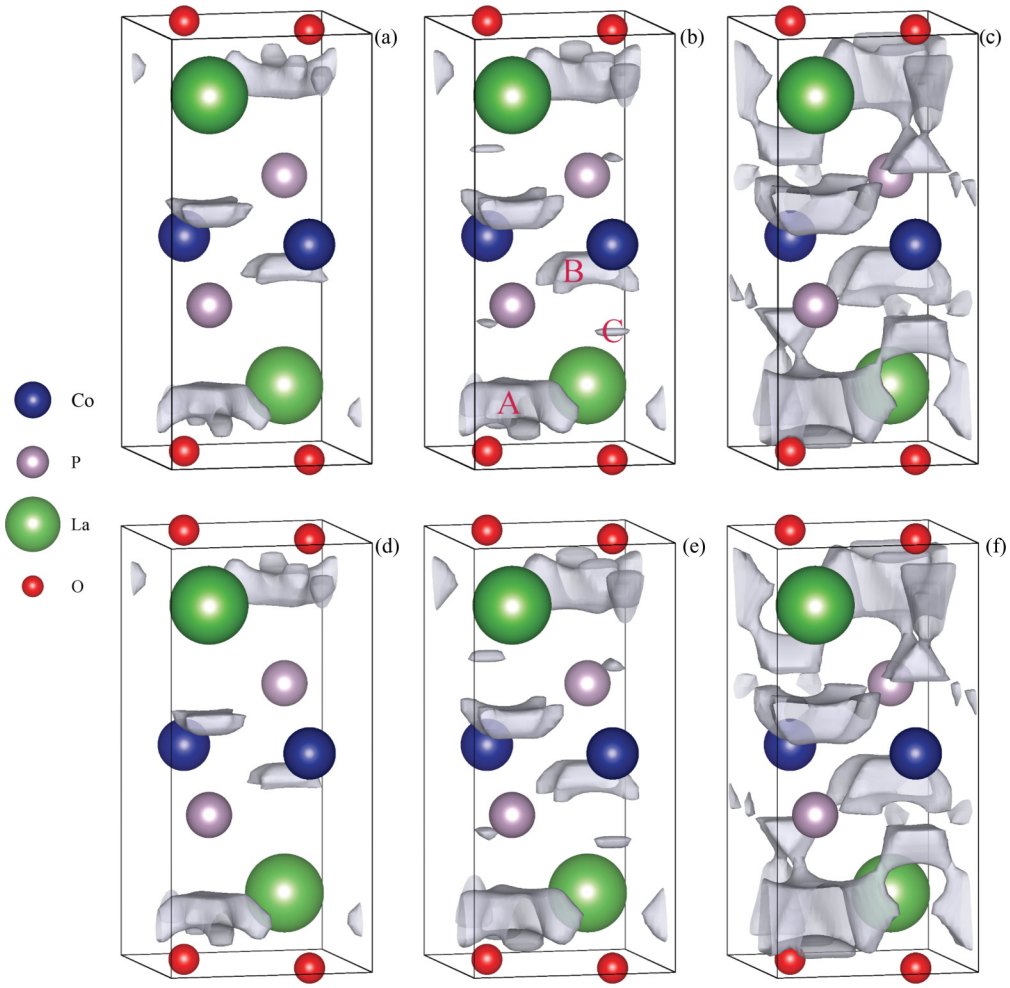

FIG. 9. (Color online) Isosurfaces of the electrostatic potential of LaCoPO for ambient P (upper panels) and $P = 30$ kbar (lower panels). For each pressure, the energies corresponding to the first eigenvalue for a muon in sites A, B), and C are shown, i.e., $V(\mathbf{r})^{\text{iso}} = E_{\text{ZP}}^{\text{A}}$ for (a) and (d); $V(\mathbf{r})^{\text{iso}} = E_{\text{ZP}}^{\text{B}}$ for (b) and (e); $V(\mathbf{r})^{\text{iso}} = E_{\text{ZP}}^{\text{C}}$ for (c) and (f).

As already mentioned, DFT calculations do not evidence structural or magnetic transitions triggered by P. The energy minima and ZP energies of the interstitial sites are slightly modified with increasing P up to 30 kbar but variations are smooth and of the order of the estimated accuracy of the calculation. The same trend shown in Table III for the energy minima and the zero-point motion is found also for higher pressures (P up to 100 kbar). Minima B and C, in particular, increase their energy with respect to site A, while the ZP energies of both the sites (with reference to the relative energy minimum) do not change significantly. This allows us to state that the occupation probability of those sites should remain practically unchanged upon increasing P or, at least, that site A turns out to be even more and more favorable from an energetic point of view in comparison with B and C. In conclusion, no evidence for sudden changes in the population of interstitial sites can be derived from DFT calculations.

After considering both the experimental and the computational results described above, the possibility of a sudden change of site occupation for μ^+ upon increasing P seems to be very unlikely. From the experimental side, in fact, no sign of occupancy of different sites is present for any of the investigated samples (see the inset of Fig. 2 for representative raw data). An unrealistically complete redistribution of the site occupation between the two inequivalent sites A and B would then be needed in order to explain the experimental results. As already stressed above, moreover, no sign of structural transitions upon increasing P for the investigated samples was evidenced by means of DFT computations. Due to the smoothness of the energy landscape coming out from calculations, then, it seems to be highly unlikely to attribute the sharp and dramatic drop in the internal field occurring at $P \simeq 5$ kbar (see the main panel of Fig. 8) to a modification in $\mathbf{r}_\mu$.

C. Computation of the perturbation effect induced by the muon

In this section, we will consider the local perturbation induced by the implanted muons. We studied the effect of μ^+-induced lattice distortion on the electrostatic potential landscape. Normally, the dielectric screening in metals is so efficient that μ^+ will not cause significant lattice distortion. However, here we are dealing with a material that is a poor metal, and so it is important to get an estimate of any lattice distortion effect. Since we need to get just an estimate, we can ignore the effect of ZP motion and treat the μ^+ as if it

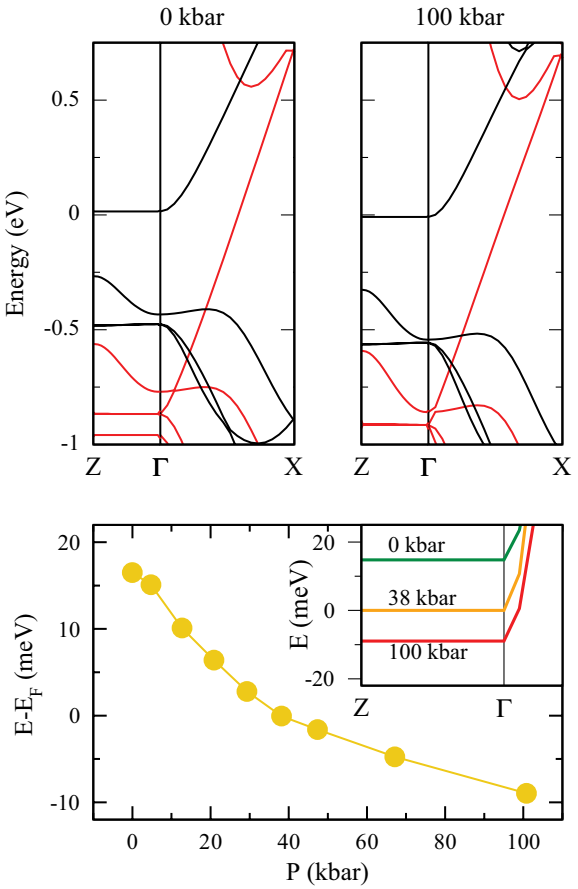

FIG. 10. (Color online) Upper panels: energy bands of LaCoPO at ambient P and at 100 kbar ($E_F = 0$). The black (red) color refers to majority (minority) spin bands. Lower panel: difference between the energy at Γ and the Fermi energy E_F for the band crossing the Fermi energy. Inset: energy band dispersion for selected P values.

were a hydrogen interstitial impurity. We model the isolated impurity within the supercell approach by building a 64-atom supercell up from our bulk structure. The supercell volume was kept constant while atomic positions were allowed to relax. μ^+ are positively charged particles but, at the same time, our supercell must have a neutral charge because the electronic screening in metals does neutralize the μ^+ charge. For the hydrogen impurity, we chose those sites identified as absolute minima by the electrostatic potential landscape. We then let the system evolve towards the GS allowing both electron rearrangement and lattice distortion. The final optimized position for the impurity represents the refined site for the μ^+, and we found that the refined μ^+ position is in agreement with the one obtained by analyzing the electrostatic potential minima. Fully relaxed structures at ambient P, at $P = 15$ and 30 kbar, show that both the μ^+ position inside the cell and the distance between μ^+ and P ions vary less than 0.04 Å. The phosphorous ion close to μ^+ is pushed closer to the Co plane by ∼0.06 Å and its four neighboring Co atoms increase their magnetic moment to 0.6 μ_B. Nevertheless, once more, no appreciable modification of the crystal structure and of the magnetic properties of the whole system (crystal and μ^+) which could in principle justify the drop of the internal field observed around $P \sim 5$ kbar could be computed as a function of P.

D. Pressure-induced effects on the energy bands

In order to identify possible changes of the spin density at the μ^+ site, we computed the band structures to evaluate the contribution of the conduction electrons to the hyperfine field as a function of pressure. At $P \sim 38$ kbar, an unoccupied electron band shifts across the Fermi energy as shown in Fig. 10, creating a large cylindrical Fermi surface owing to the flat dispersionless band along Γ-Z shown in figure. This modification in the band structure strongly suggests that the variation of the local field upon increasing P can be due to a change in the transferred hyperfine contact field $\mathbf{B}_c(\mathbf{r}_\mu)$ reported in Eq. (4), strongly influenced by the conduction electrons.[53] It should be remarked that, according to what is reported in Table III, for the in-plane orientation of the spins one has $\mathbf{B}_{dip}[\mathbf{r}_\mu(A)] = -\mathbf{B}_L$ and the muon in site A is thus subject only to the contribution of $\mathbf{B}_c(\mathbf{r}_\mu)$.

V. DISCUSSION

Both chemical and external pressure have been shown to affect the ferromagnetic properties of the Co-based 1111 oxypnictides. ZF-μ^+SR experiments display that the magnetic ordering temperature T_c increases as a function of pressure. The internal field at the muon site B_μ is found to abruptly decrease around 5 kbar in LaCoPO. A change of the same amount is found when lanthanum is substituted by smaller Pr ions. This demonstrates that chemical pressure mimics the hydrostatic pressure as can be deduced from Fig. 8. Claims of close analogies among the effect of chemical and external pressures were already reported concerning both 1111 and 122 compounds.[38–40] In order to understand the origin of the drastic reduction observed for B_μ, we have investigated the behavior of those quantities, implicitly included in Eq. (4), that mainly contribute to the precession frequency of the muon around the local field, namely, the Co-ordered magnetic moment μ_{Co} and both the distance and the density of the spin at the μ^+ site as a function of P.

Magnetization measurements have shown no significative change of μ_{Co} either by changing chemical or external pressure (see the inset of Fig. 7). DFT calculations have been performed in order to determine the muon sites and display that only two lattice positions are stable, namely, close to the CoP (site A) and to the RO (site B) layers (Fig. 9), the latter being energetically favored. Since ZF-μ^+SR display only one oscillating component, only one site is really occupied. The calculation of electrostatic potentials does not display any strong variation as a function of pressure, indicating that the μ^+ site can not change. Since also μ_{Co} is constant, we can conclude that neither the dipolar interaction nor the Lorenz field of Eq. (4) can be responsible for the suppression of the local field at the μ^+ site as a function of pressure. On the other hand, DFT band-structure calculations show that a slight variation in the energy of a minority band occurs as a function of pressure, displaying that a crossing of the Fermi level takes place around 38 kbar, as shown in Fig. 10. This computational outcome suggests a sudden change of the hyperfine contribution in

Eq. (4) due to the occupation of this minority spin band. A notable discrepancy between the critical P value for the drop of the internal field from experimental (∼5 kbar) and DFT (∼38 kbar) results is found. This difference may be understood by considering that, first, the band structure is extremely sensitive to the position of the P ions. The shift of the position of P ions towards the Co plane introduced by the incoming μ^+ discussed above is not taken into account when inspecting the band structure and it may indeed favor the population of the unoccupied valence band at lower P values. In addition, in this delicate scenario, even small nonhydrostatic effects not taken into account in the calculations can shift the critical pressure. Moreover, the DFT approach for the first-principles analysis may underestimate P effects as a consequence of the overestimated magnetic moment, which in turn is related to the height of phosphorous ions.[54] Unfortunately, as already recalled above, no experimental structural refinements as a function of P are available at the moment. Thus, we can not quantify the mismatch between DFT obtained and real crystal structures as a function of pressure.

Other hypotheses can be made in order to explain the observed phenomenology by referring to the intrinsic magnetic properties of the materials, whose changes upon increasing P can be directly reflected in relative modifications into one (or more) terms appearing in Eq. (4). One can then take into consideration the possibility of a P-triggered reorienting of the FM configuration. The values for the modification of the overall local magnetic field at the muon site according to this hypothesis are provided in Table III. Aside from a possibly satisfying explanation of experimental data from a quantitative point of view, this hypothesis should be considered as unrealistic mainly due to the low absolute value of spin-orbit interaction for the Co ions. The different energies of the GSs were analyzed by performing noncollinear spin-polarized calculations for different P and easy magnetization axes orientations. The results for different spin configurations are found to be nearly degenerate so that, in conclusion, the mean-field approach does not provide a clue to support this alternative.

VI. CONCLUSIONS

We performed detailed measurements by means of muon spin spectroscopy on LaCoPO, PrCoPO, and LaCoAsO under applied hydrostatic pressure. The localized electrons on the ionic shells of Pr^{3+} ions do not affect at all the local static features of magnetism as detected by muons in spite of the high value of the magnetic moment expected for the free Pr^{3+} ion. Phosphorous-based compounds turn out to be much more sensitive than LaCoAsO to the application of pressure. In particular, the critical transition temperature to the ferromagnetic phase in LaCoPO is sizably increased both by chemical and external pressures (the former being triggered by the full Pr^{3+}/La^{3+} substitution), while for LaCoAsO the effect is also present but by far less marked. The increase of both kinds of pressure, moreover, dramatically suppresses the local magnetic field at the muon site leaving the magnetic moment per Co ion substantially unchanged. Density-functional-theory calculations of the band structure suggest that this change of the muon field is due to a subtle change of the hyperfine coupling driven by a minority band crossing the Fermi surface. Results clearly evidence how crucial the role of pressure is on the properties of the ferromagnetic phase and, at the same time, how similar the effects of chemical and external hydrostatic pressure is in 1111 oxypnictide compounds. A computational description of LaCoPO performed by means of *ab initio* DFT calculations supports these findings and suggests that chemical and external pressures both trigger a qualitative change in the electronic band structure of the investigated compounds.

ACKNOWLEDGMENTS

G. Prando acknowledges support from the Leibniz-Deutscher Akademischer Austauschdienst (DAAD) Post-Doc Fellowship Program. G. Profeta acknowledges support from the FP7 European project SUPER-IRON (Grant Agreement No. 283204), by a CINECA-HPC ISCRA grant, and by an HPC grant at CASPUR. F.B. acknowledges support from CASPUR under the Standard HPC Grant 2012 and from the FP7 European project SUPER-IRON (Grant Agreement No. 283204). E.M.B. and H.-J.G. acknowledge support from Deutsche Forschungsgemeinschaft (DFG) through SPP1458 (Grant No. GR3330/2). P.C. and S.S. acknowledge support from Fondazione Cariplo (research Grant No. 2011-0266). The structural models in the figures were rendered using the VESTA package.[55]

*g.prando@ifw-dresden.de

[1] Y. Kamihara, T. Watanabe, M. Hirano, and H. Hosono, J. Am. Chem. Soc. **130**, 3296 (2008).
[2] D. C. Johnston, Adv. Phys. **59**, 803 (2010).
[3] Z.-A. Ren, W. Lu, J. Yang, W. Yi, X.-L. Shen, Z.-C. Li, G.-C. Che, X.-L. Dong, L.-L. Sun, F. Zhou, and Z.-X. Zhao, Chin. Phys. Lett. **25**, 2215 (2008).
[4] G. Prando, A. Lascialfari, A. Rigamonti, L. Romanó, S. Sanna, M. Putti, and M. Tropeano, Phys. Rev. B **84**, 064507 (2011).
[5] A. S. Sefat, A. Huq, M. A. McGuire, R. Jin, B. C. Sales, D. Mandrus, L. M. D. Cranswick, P. W. Stephens, and K. H. Stone, Phys. Rev. B **78**, 104505 (2008).
[6] A. Marcinkova, D. A. M. Grist, I. Margiolaki, T. C. Hansen, S. Margadonna, and Jan-Willem G. Bos, Phys. Rev. B **81**, 064511 (2010).
[7] V. P. S. Awana, A. Pal, A. Vajpayee, R. S. Meena, H. Kishan, M. Husain, R. Zeng, S. Yu, K. Yamaura, and E. Takayama-Muromachi, J. Appl. Phys. **107**, 09E146 (2010).
[8] T. Shang, L. Yang, Y. Chen, J. L. Zhang, L. Jiao, J. Chen, J. Dai, and H. Q. Yuan, arXiv:1212.0221.
[9] T. Shang, L. Yang, N. Cornell, F. Ronning, Y. Chen, L. Jiao, J. Chen, A. Howard, J. D. Thompson, A. Zakhidov, M. B. Salamon, and H. Q. Yuan, arXiv:1212.0222.
[10] A. S. Sefat, R. Jin, M. A. McGuire, B. C. Sales, D. J. Singh, and D. Mandrus, Phys. Rev. Lett. **101**, 117004 (2008).

[11] A. Yamamoto, J. Jaroszynski, C. Tarantini, L. Balicas, J. Jiang, A. Gurevich, D. C. Larbalestier, R. Jin, A. S. Sefat, M. A. McGuire, B. C. Sales, D. K. Christen, and D. Mandrus, Appl. Phys. Lett. **94**, 062511 (2009).
[12] G. Prando, R. Giraud, M. Abdel-Hafiez, S. Aswartham, A. U. B. Wolter, S. Wurmehl, and B. Büchner, arXiv:1207.2457.
[13] H. Maeter, J. E. Hamann-Borrero, T. Goltz, J. Spehling, A. Kwadrin, A. Kondrat, L. Veyrat, G. Lang, H.-J. Grafe, C. Hess, G. Behr, B. Büchner, H. Luetkens, C. Baines, A. Amato, N. Leps, R. Klingeler, R. Feyerherm, D. Argyriou, and H.-H. Klauss, arXiv:1210.6959.
[14] G. Prando, P. Carretta, A. Rigamonti, S. Sanna, A. Palenzona, M. Putti, and M. Tropeano, Phys. Rev. B **81**, 100508(R) (2010).
[15] H. Maeter, H. Luetkens, Y. G. Pashkevich, A. Kwadrin, R. Khasanov, A. Amato, A. A. Gusev, K. V. Lamonova, D. A. Chervinskii, R. Klingeler, C. Hess, G. Behr, B. Büchner, and H.-H. Klauss, Phys. Rev. B **80**, 094524 (2009).
[16] R. De Renzi, P. Bonfà, M. Mazzani, S. Sanna, G. Prando, P. Carretta, R. Khasanov, A. Amato, H. Luetkens, M. Bendele, F. Bernardini, S. Massidda, A. Palenzona, M. Tropeano, and M. Vignolo, Supercond. Sci. Technol. B **25**, 084009 (2012).
[17] H. Yanagi, R. Kawamura, T. Kamiya, Y. Kamihara, M. Hirano, T. Nakamura, H. Osawa, and H. Hosono, Phys. Rev. B **77**, 224431 (2008).
[18] H. Ohta and K. Yoshimura, Phys. Rev. B **79**, 184407 (2009).
[19] H. Ohta and K. Yoshimura, Phys. Rev. B **80**, 184409 (2009).
[20] H. Ohta, C. Michioka, A. Matsuo, K. Kindo, and K. Yoshimura, Phys. Rev. B **82**, 054421 (2010).
[21] H. Ohta, C. Michioka, and K. Yoshimura, J. Phys. Soc. Jpn. **79**, 054703 (2010).
[22] R. Sarkar, A. Jesche, C. Krellner, M. Baenitz, C. Geibel, C. Mazumdar, and A. Poddar, Phys. Rev. B **82**, 054423 (2010).
[23] V. P. S. Awana, I. Nowik, A. Pal, K. Yamaura, E. Takayama-Muromachi, and I. Felner, Phys. Rev. B **81**, 212501 (2010).
[24] A. Pal, M. Tropeano, S. D. Kaushik, M. Hussain, H. Kishan, and V. P. S. Awana, J. Appl. Phys. **109**, 07E121 (2011).
[25] H. Ohta, C. Michioka, and K. Yoshimura, Phys. Rev. B **84**, 134411 (2011).
[26] J. Sugiyama, M. Mansson, O. Ofer, K. Kamazawa, M. Harada, D. Andreica, A. Amato, J. H. Brewer, E. J. Ansaldo, H. Ohta, C. Michioka, and K. Yoshimura, Phys. Rev. B **84**, 184421 (2011).
[27] C. Krellner, U. Burkhardt, and C. Geibel, Phys. B (Amsterdam) **404**, 3206 (2009).
[28] A. Pal, S. S. Mehdi, M. Husain, B. Gahtori, and V. P. S. Awana, J. Appl. Phys. **110**, 103913 (2011).
[29] M. Majumder, K. Ghoshray, A. Ghoshray, B. Bandyopadhyay, B. Pahari, and S. Banerjee, Phys. Rev. B **80**, 212402 (2009).
[30] H. Sugawara, K. Ishida, Y. Nakai, H. Yanagi, T. Kamiya, Y. Kamihara, M. Hirano, and H. Hosono, J. Phys. Soc. Jpn. **78**, 113705 (2009).
[31] M. Majumder, K. Ghoshray, A. Ghoshray, B. Bandyopadhyay, and M. Ghosh, Phys. Rev. B **82**, 054422 (2010).
[32] M. Majumder, K. Ghoshray, A. Ghoshray, A. Pal, and V. P. S. Awana, J. Phys. Soc. Jpn. **81**, 054702 (2012).
[33] E. M. Brüning, C. Krellner, M. Baenitz, A. Jesche, F. Steglich, and C. Geibel, Phys. Rev. Lett. **101**, 117206 (2008).
[34] Y. Luo, Y. Li, S. Jiang, J. Dai, G. Cao, and Z.-A. Xu, Phys. Rev. B **81**, 134422 (2010).
[35] R. Sarkar, M. Baenitz, A. Jesche, C. Geibel, and F. Steglich, J. Phys.: Condens. Matter **24**, 135602 (2012).
[36] A. Jesche, T. Förster, J. Spehling, M. Nicklas, M. de Souza, R. Gumeniuk, H. Luetkens, T. Goltz, C. Krellner, M. Lang, J. Sichelschmidt, H.-H. Klauss, and C. Geibel, Phys. Rev. B **86**, 020501(R) (2012).
[37] N. Colonna, G. Profeta, and A. Continenza, Phys. Rev. B **83**, 224526 (2011).
[38] S. A. J. Kimber, A. Kreyssig, Y.-Z. Zhang, H. O. Jeschke, R. Valentí, F. Yokaichiya, E. Colombier, J. Yan, T. C. Hansen, T. Chatterji, R. J. McQueeney, P. C. Canfield, A. I. Goldman, and D. N. Argyriou, Nat. Mater. **8**, 471 (2009).
[39] G. Prando, S. Sanna, G. Lamura, T. Shiroka, M. Tropeano, A. Palenzona, H.-J. Grafe, B. Büchner, P. Carretta, and R. De Renzi, Phys. Status Solidi B (2013), doi: 10.1002/pssb.201200767.
[40] E. Gati, S. Köhler, D. Guterding, B. Wolf, S. Knöner, S. Ran, S. L. Bud'ko, P. C. Canfield, and M. Lang, Phys. Rev. B **86**, 220511(R) (2012).
[41] F. Nitsche, A. Jesche, E. Hieckmann, T. Doert, and M. Ruck, Phys. Rev. B **82**, 134514 (2010).
[42] A. Yaouanc and P. Dalmas de Réotier, *Muon Spin Rotation, Relaxation, and Resonance: Applications to Condensed Matter* (Oxford University Press, Oxford, UK, 2011).
[43] R. Khasanov, S. Sanna, G. Prando, Z. Shermadini, M. Bendele, A. Amato, P. Carretta, R. De Renzi, J. Karpinski, S. Katrych, H. Luetkens, and N. D. Zhigadlo, Phys. Rev. B **84**, 100501(R) (2011).
[44] W. J. Duncan, O. P. Welzel, C. Harrison, X. F. Wang, X. H. Chen, F. M. Grosche, and P. G. Niklowitz, J. Phys.: Condens. Matter **22**, 052201 (2010).
[45] J. Sugiyama, Y. Ikedo, K. Mukai, J. H. Brewer, E. J. Ansaldo, G. D. Morris, K. H. Chow, H. Yoshida, and Z. Hiroi, Phys. Rev. B **73**, 224437 (2006).
[46] V. H. Tran, P. Rogl, P. Dalmas de Réotier, and A. Yaouanc, Phys. Rev. B **83**, 144417 (2011).
[47] S. Barth, E. Albert, G. Heiduk, A. Möslang, A. Weidinger, E. Recknagel, and K. H. J. Buschow, Phys. Rev. B **33**, 430 (1986).
[48] G. Kresse and J. Furthmüller, Phys. Rev. B **54**, 11169 (1996).
[49] ELK code (version 1.4.18), http://elk.sourceforge.net.
[50] J. P. Perdew, K. Burke, and M. Ernzerhof, Phys. Rev. Lett. **77**, 3865 (1996).
[51] P. E. Blöchl, Phys. Rev. B **50**, 17953 (1994).
[52] H. J. Monkhorst and J. D. Pack, Phys. Rev. B **13**, 5188 (1976).
[53] C. P. Slichter, *Principles of Magnetic Resonance* (Springer, Berlin, 1990).
[54] Y.-Z. Zhang, H. C. Kandpal, I. Opahle, H. O. Jeschke, and R. Valentí, Phys. Rev. B **80**, 094530 (2009).
[55] K. Momma and F. Izumi, J. Appl. Cryst. **44**, 1272 (2011).